Convective growth of cyclotron harmonic waves on a bounded coaxial electron beam

J. L. Hirshfield and Changbiao Wang
Department of Physics, Yale University, P. O. Box 6666, New Haven, Connecticut 06511-8167
(Received 3 October 1994)

Analysis and numerical evaluations are presented for the spatial growth of small-signal modified electron Bernstein waves that stand radially and propagate axially along a beam-filled coaxial waveguide. It is shown that these waves, when coupled strongly to fields of an electromagnetic TE_{11} mode in the interior cylindrical waveguide of this configuration, can make possible an amplifier of cyclotron harmonic waves that would possess several unique properties. In particular, millimeter wavelength amplifiers based on this interaction would require neither high magnetic fields nor high electron beam voltages, and thus would not require the bulky superconducting magnets and highly insulated high voltage power supplies usually associated with fast-wave gyro devices. The analysis extends prior work on interactions of this type, including in the calculations simultaneous contributions from more than one term in the infinite series dispersion relation. Effects of finite axial beam velocity spread on the gain and bandwidth characteristics of the interaction are also calculated, thereby accounting for the irreducible velocity spreads attributable to space charge potential depression on the beam.

PACS number(s): 42.52.+x, 41.75.−i, 52.75.Ms, 52.35.Hr

I. INTRODUCTION

This paper presents results of analysis and numerical evaluations describing the spatial growth of small-signal modified electron Bernstein waves [1] that stand radially and propagate axially along a beam-filled coaxial waveguide. This arrangement is at the heart of an amplifier concept that would require neither high electron beam voltages nor high guide magnetic fields for operation at millimeter wavelengths [2]. An abbreviated description for a related amplifier using a beam-filled cylindrical waveguide has been previously published [3]. The beam excitations are labeled "modified" electron Bernstein waves because they are characterized principally by short-wavelength beam perturbations directed across the magnetic field that guides the beam. But the excitations also possess long-wavelength perturbations directed along the guide field, a feature not normally associated with Bernstein waves. The principal objective of the present work is to explore the linearized version of this interaction in coaxial geometry where, as shall be shown below, advantages exist over cylindrical geometry for a practical amplifying device. In addition, results are given for the influence on gyroharmonic linear wave growth from contributions of harmonic terms in the infinite series dispersion relation that are adjacent to the harmonic term of interest and from finite axial beam velocity spread.

Nearly 15 years ago, the possibility of exploiting the instability of radially standing Bernstein modes on electron beams for generating millimeter wave radiation was demonstrated analytically [4,5] and experimentally [6]. Published experiments showed coherent oscillations up to 62 GHz at the fourth gyroharmonic, using a 15-kV low current beam in a quasioptical resonator. Further experiments [7] showed oscillations up to 311 GHz at the eighth gyroharmonic in a two-cavity quasioptical configuration. None of the high harmonic results could be explained without invoking a growth mechanism for unstable electrostatic modes on the electron beam. Recently, Li and Antonsen [8] have reviewed and extended the analysis of this mechanism to describe coupling between electron Bernstein modes and electromagnetic modes of gyrotron cavities and to investigate degradation in beam quality that might result from the electrostatic instability.

In order to produce gyroharmonic amplification of radiation at a wavelength of 1 mm, a guide magnetic field of strength about $107\gamma/n$ kG must be employed, where γ is the relativistic energy factor and n is the harmonic index. But if practical limitations require the device to employ noncryogenic magnet coils and to be lightweight, it is apparent that n/γ must have a value of at least 10. Fast-wave gyroharmonic interactions in smooth-wall circuits utilizing electron beams with harmonic indices n above 2 or 3 usually demand beam energies of the order of 100 kV, since harmonic coupling is a strongly relativistic effect that increases as beam energy increases. But there is ample experimental evidence for the existence of interactions at very high gyroharmonics in low energy laboratory and ionospheric plasmas. For example, Landauer [9] reported observation of about 40 harmonics in noise emission from low pressure gas discharges; Crawford, Kino, and Weiss observed about ten harmonic resonances in microwave transmission across a plasma column [10]; and multiple harmonic interactions in ionospheric topside soundings have been reported [11]. No theory based solely on electromagnetic interactions in weakly relativistic plasmas has been able to explain these observations. But, if slow electrostatic waves standing across the guide magnetic field (counterpropagating electron Bernstein waves) can be supported by the beam or plasma and if conditions for excitation of these waves can be found, then dynamical effects that are essentially rela-

tivistic can occur for low energy beams and plasmas. This follows since the ratio of the mean electron gyration radius to the electrostatic wavelength will not be a quantity much less than unity. Detailed models invoking this concept have served to explain in detail the plasma observations [9–11] and the millimeter wave beam oscillations [6,7].

This paper is organized as follows. Section II describes the electrostatic fields of a coaxial waveguide containing a uniform electron beam; both static and oscillatory fields are discussed: the static (space charge) field can be used to estimate the axial velocity spread to be expected for a given beam perveance due to potential depression, while the oscillatory modes dictate the spectrum of transverse wave numbers that are to be included in the analysis of wave dispersion and growth. Section III gives an analysis of the Harris linearized dispersion relation [12] appropriate to steady-state waves with the aforementioned spectrum of real transverse wave numbers, propagating with possible growth or decay along the coaxial waveguide. Section IV gives results of numerical evaluations for spatial growth rates for such waves, including contributions from nearest-neighbor terms in the infinite-series dispersion relation and effects due to finite axial velocity spread on the beam. Section V describes a conceptual device design for an amplifier showing a possible means of input-output coupling and mode selectivity. Section VI contains a summary of the important results of this work and suggestions for additional study.

II. ELECTROSTATIC FIELDS IN A COAXIAL BEAM-FILLED WAVEGUIDE

We consider an axially uniform coaxial waveguide bounded by perfectly conducting cylinders with radii R_1 and R_2, where $R_2 > R_1$. For excitations at frequency ω with spatial variations having scale lengths much less than the free-space wavelength $2\pi c/\omega$, the full set of Maxwell's field equations for the system can be approximated by Poisson's equation for the electrostatic potential $\phi(r,\theta,z,t)$,

$$\nabla^2\phi(r,\theta,z,t) = -en(r,\theta,z,t)/\varepsilon_0 \tag{1}$$

with the corresponding electric field $\mathbf{E}(r,\theta,z,t) = -\nabla\phi(r,\theta,z,t)$. Here e is the magnitude of the electron charge, ε_0 is the permittivity of free space, and $n(r,\theta,z,t)$ is the electron concentration in the beam, as a function of time t and cylindrical space coordinates (r,θ,z). The beam current is assumed to be small enough to allow neglect of static self-magnetic fields and $\mathbf{E}(r,\theta,z,t)$ is obviously curl free. For harmonic steady-state excitations,

$$\phi(r,\theta,z,t) = \sum_{m,s} \phi_{ms}(r,\theta)\exp[i(k_{zms}z - \omega t)] . \tag{2}$$

In Eq. (2) the double sum is over modes with distinctive radial (labeled s) and azimuthal (labeled m) eigenvalues and the radian frequency ω is real. Each individual mode (m,s) has one or more possibly complex axial wavenumbers k_{zms}.

The static field profile is given for the case $m=s=0$, with $\omega = k_{z00} = 0$. We assume the beam density $n(r,\theta) = n_0$ to be constant and assume the guide magnetic field to be strong enough to effect laminar confined flow. In this case the potential, as given by a solution of Eq. (1), is

$$\phi(r,\theta) = \phi(r) = \frac{n_0 e}{4\varepsilon_0}\left[(r^2 - R_1^2) - (R_2^2 - R_1^2)\frac{\ln(r/R_1)}{\ln(R_2/R_1)}\right] , \tag{3}$$

where the boundary conditions are taken to be $\phi(R_1) = \phi(R_2) = 0$. To find the potential depression $-(\Delta\phi)_{\text{coax}}$, defined as the largest negative value of $\phi(r)$, one differentiates Eq. (3) with respect to r and sets the result equal to zero. This gives the location of the potential minimum at $r = R_1[(\mu-1)/\ln\mu]^{1/2}$, from which it follows that

$$(\Delta\phi)_{\text{coax}} = \frac{n_0 e R_1^2}{4\varepsilon_0}\left[\frac{\mu-1}{\ln\mu} - 1 - \frac{\mu-1}{\ln\mu}\ln\left[\frac{\mu-1}{\ln\mu}\right]\right] , \tag{4}$$

where $\mu = R_2^2/R_1^2$. The potential depression for a cylindrical beam is $(\Delta\phi)_{\text{cyl}} = n_0 e R_2^2/4\varepsilon_0$, so that $(\Delta\phi)_{\text{coax}} = (\Delta\phi)_{\text{cyl}} F(\mu)$, where

$$-F(\mu) = \frac{1}{\mu\ln\mu}\left[\mu - 1 - \ln\mu - (\mu-1)\ln\left[\frac{\mu-1}{\ln\mu}\right]\right] . \tag{5}$$

The quantity $F(\mu)$, a plot of which is shown in Fig. 1, is the factor by which the magnitude of the potential depression for a coaxial beam is lower than that for a cylindrical beam of equal charge density. With $R_2 = 4R_1$, for example, one has $F(\mu) = 0.295$.

To estimate the magnitude of axial velocity spread across a gyrating beam caused by potential depression,

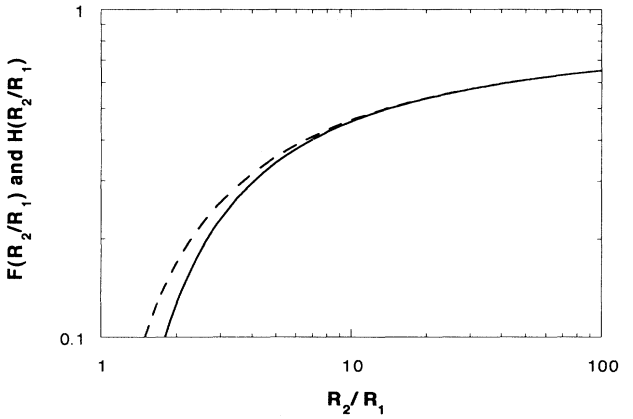

FIG. 1. Space charge depression reduction factors $F(\mu)$ and $H(\mu)$ versus $R_2/R_1 = \mu^{1/2}$ for a coaxial bounded beam. $F(\mu)$ (solid curve) is the reduction in potential depression and $H(\mu)$ (dashed curve) is the reduction in axial velocity spread for a coaxial beam, as compared with a cylindrical beam with radius R_2 of equal perveance.

one introduces the ratio of transverse-to-axial velocity $v_\perp/v_z=\alpha$ and the relativistic energy factor $\gamma=1+eV/mc^2$, where V is the voltage through which the beam has been accelerated. One then has $v_z=c[(1-\gamma^{-2})/(1+\alpha^2)]^{1/2}$. In terms of the beam current $I=\pi n_0 e v_z(R_2^2-R_1^2)$, it follows that

$$\frac{\Delta v_z}{v_z}=\frac{1}{8\pi\varepsilon_0}\left[\frac{m}{2e}\right]^{1/2}(1+\alpha^2)^{1/2}H(\mu)\hat{P}$$
$$=7.58\times10^3(1+\alpha^2)^{1/2}H(\mu)\hat{P}\ , \quad (6)$$

where $\hat{P}=(I/V^{3/2})[2/(1+\gamma)]^{3/2}$ A/V$^{3/2}$ is a generalized beam perveance and $H(\mu)=[\mu F(\mu)/(\mu-1)]$. For a cylindrical beam, $H(\mu)=1$, so that this quantity is seen to give the reduction in axial velocity spread that results when a coaxial beam is used in place of a cylindrical beam of equal perveance. The factor $H(\mu)$ is also plotted in Fig. 1. As an example, if $R_2=4R_1$, the reduction factor $H(\mu)$ is seen to be 0.315. Thus one advantage of employing a coaxial rather than a cylindrical beam (of equal perveance) is the markedly smaller axial velocity spread for the former that will be caused by beam space charge.

If the beam is produced using convergent flow the above analysis is invalid, since azimuthal particle motions (as in Brillouin flow [13]) will induce a nonuniform radial density profile, resulting in an axial velocity spread (even in the absence of scalloping) that can be smaller than that given by Eq. (6). However, for purposes of the present work, the prediction of Eq. (6) will be taken as a conservative upper limit for the axial velocity spread on the beam.

Eigenfunctions in Eq. (2) for $s\neq0$ and $m\neq0$ are given by

$$\phi_{ms}(r,\theta)=[A_{ms}J_m(k_{\perp ms}r)+B_{ms}Y_m(k_{\perp ms}r)]\cos m\theta \quad (7)$$

and a similar form proportional to $\sin m\theta$. In Eq. (7) J_m and Y_m are Bessel functions of mth order of the first and second kinds and A_{ms} and B_{ms} are constants. The excitations given by Eq. (7) are oftimes referred to as Gould-Trivelpiece modes [14]. In a prior discussion of the amplifying mechanism for Bernstein modes on cylindrical beams (where $B_{ms}=0$), the monopole mode ($m=0$) was analyzed [3]. For the coaxial case, injection of an input signal using the TE_{11} electromagnetic mode within the cylindrical inner pipe of radius R_1 suggests itself. We assume that coupling between electromagnetic fields within $0\leq r\leq R_1$ and electrostatic fields within $R_1\leq r\leq R_2$ can be azimuthally selective, through the use of judiciously placed coupling slots so as to eliminate all oscillatory fields except for those in Eq. (7) with $m=1$. This point will be discussed in Sec. V. The eigenfunction for the fields within the beam to be analyzed here is thus selected to be

$$\phi_s(r,\theta)=[A_sJ_1(k_{\perp s}r)+B_sY_1(k_{\perp s}r)]\cos\theta \quad (8)$$

while the eigenvalues $k_{\perp s}$, found from setting $\phi_s(R_1,\theta)=\phi_s(R_2,\theta)=0$, are given by the roots of

$$J_1(k_{\perp s}R_1)Y_1(k_{\perp s}R_2)=J_1(k_{\perp s}R_2)Y_1(k_{\perp s}R_1)\ . \quad (9)$$

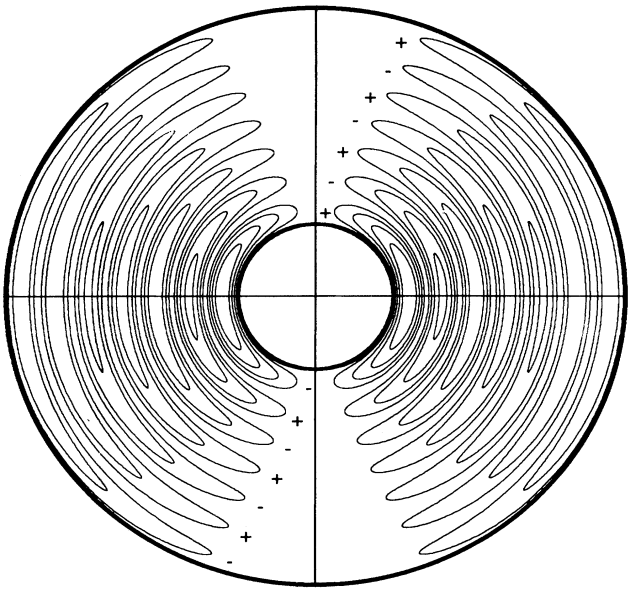

FIG. 2. Equipotentials for the seventh radial dipole mode for a uniform beam within coaxial conducting cylinders. Curves shown are for normalized equipotentials equal to 0.2, 0.4, 0.6, and 0.8 of the maximum potential (for the inner two lobes); 0.2, 0.4, and 0.6 (next three lobes); and 0.2 and 0.4 (outer two lobes).

An approximate series representation for the allowed eigenvalues given by Eq. (9) can be found [15]. For example, with $R_2=4R_1$,

$$k_{\perp s}R_1\approx1.0472s+0.089\,53s^{-1}-0.046\,88s^{-3}+\cdots\ . \quad (10)$$

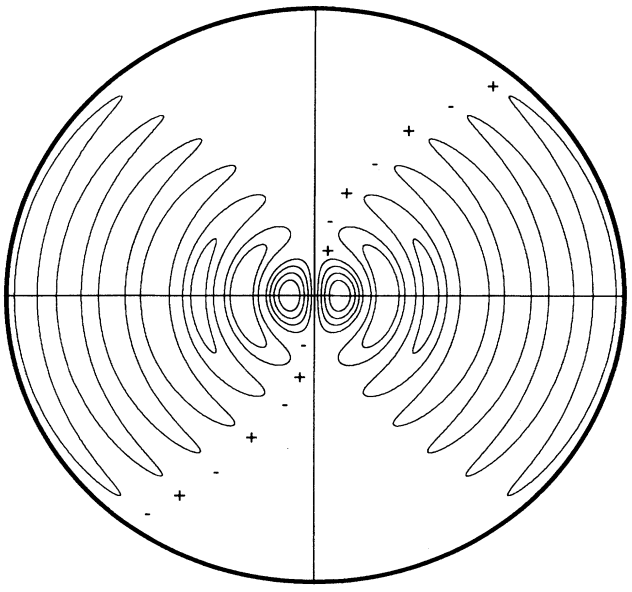

FIG. 3. Equipotentials for the seventh radial dipole mode for a uniform beam within a single conducting cylinder. Curves shown are for normalized potentials equal to 0.2, 0.4, 0.6, and 0.8 of the maximum potential (inner lobe); 0.2 and 0.4 (next two lobes); and 0.2 (outer four lobes).

Equation (10) is accurate to better than one part in 10^5 for $s > 7$.

Equipotentials for the mode $s = 7$ are depicted in Fig. 2 for the case $R_2 = 4R_1$, where the contours shown are for potential values in increments of 20% of the maximum value. (The mode $s = 7$ is chosen for illustration, rather than a higher-s mode, merely to avoid undue crowding in Figs. 2 and 3.). For comparison, corresponding equipotentials for the cylindrical case ($R_1 = 0$) are shown in Fig. 3. The concentration of high electric field (crowding together of equipotentials) near the axis for the cylindrical case, where no external access exists, is apparent. In contrast, the fields fall off more gently with radius for the coaxial case and are relatively strong near $r = R_1$, where coupling through slots to electromagnetic fields in the inner waveguide is possible.

The above analysis, based solely on the solutions of Poisson's equation for a uniform coaxial electron beam bounded by conducting cylinders, provides a prescription for finding the discrete spectrum of allowed (real) transverse wave numbers $k_{\perp s}$. The corresponding spectrum of (possibly complex) axial wave numbers k_{zs} for (possibly growing) waves at frequency ω must be determined by appeal to a governing plasma wave dispersion relation. This is undertaken in the following section.

III. ELECTROSTATIC WAVE DISPERSION AND GROWTH

For electrostatic waves in a uniform electron plasma permeated by a uniform guide magnetic field B aligned along the z axis, wave numbers and frequencies for plane waves are connected by the infinite series Harris dispersion relation [12]

$$1 = -\frac{2\pi e^2}{m\varepsilon_0}\int_0^\infty dw \int_{-\infty}^{\infty} du \sum_{n=-\infty}^{\infty} \frac{J_n^2(k_{\perp s}w/\gamma\Omega)}{k^2(\omega - n\Omega - k_{zs}u/\gamma)}\left[n\gamma\Omega\frac{\partial f_0}{\partial w} + k_{zs}w\frac{\partial f_0}{\partial u}\right], \tag{11}$$

where $f_0(u,w)$ is the distribution function for the beam electrons that is assumed to be axisymmetric in momentum space, u and w are the electron momentum components (divided by the electron rest mass) along and across B, $\Omega = eB/m\gamma$ is the relativistic gyrofrequency, J_n is the nth-order Bessel function of the first kind, $\gamma = [1 + (u^2 + w^2)/c^2]^{1/2}$ is the relativistic energy factor, $k^2 = k_{\perp s}^2 + k_{zs}^2$, and the summation over n indicates that interactions occur near all harmonics of the electron gyrofrequency Ω. An excitation at frequency ω is shown by Eq. (11) to involve the three indices (s,m,n), corresponding to the spatial parity (radial and azimuthal) of the wave potential and to the dominant term in the series in Eq. (11) corresponding to response near the nth gyroharmonic. But, as will be seen, there are circumstances where several terms under the sum in Eq. (11) may make significant contributions to wave growth at a given frequency ω. This would imply the existence of several waves of the same frequency, but usually differing perpendicular (complex) axial wave numbers. The consequences of this state of affairs will be discussed below.

The use of Eq. (11), derived for plane waves, for excitations as given by Eq. (8) needs to be clarified, since the fields are not exactly periodic in r. However, as will be seen below, the range of $k_{\perp s}r \equiv y$ within which wave growth is significant is much greater than unity. In this limit, $J_1(y) \to (2/y)^{1/2}\cos(y - 3\pi/4)$ and $Y_1(y) \to (2/y)^{1/2}\sin(y - 3\pi/4)$. Thus, for $y \gg 1$, it is seen that assuming the waves to be periodic in r is a reasonable approximation and application of Eq. (11) to these excitations can be justified.

The strength of wave-particle coupling near harmonic gyroresonance $\omega = n\Omega$ is governed by the Bessel function $J_n(x)$ in Eq. (11), whose magnitude is much smaller than unity unless its argument x is comparable to its order n. For conventional fast-wave interactions the argument $x = k_{\perp s}w/\gamma\Omega \approx n(ck_{\perp s}/\omega)(w/\gamma c) \ll n$ since, except for highly relativistic electrons, $w/\gamma c \ll 1$ and $ck_{\perp s}/\omega$ is less than unity. As a result, high gyroharmonic interactions are often weak. However, for slow electrostatic waves (equivalent to $ck_{\perp s}/\omega \gg 1$), the high harmonic interactions can be significant even for $w/\gamma c \ll 1$. It is this fact that makes electrostatic waves potent candidates for a high gyroharmonic amplifier without need for highly relativistic beam energies.

For the analysis that is to follow, it is convenient to work from the version of Eq. (11) that results from integration by parts on both u and w, namely,

$$1 = \frac{2\pi e^2}{m\varepsilon_0}\int_0^\infty dw \int_{-\infty}^{\infty} du\, f_0(u,w) \sum_{n=-\infty}^{\infty} \frac{1}{k^2}\left\{\frac{nk_{\perp s}[J_n^2(k_{\perp s}w/\gamma\Omega)]'}{(\omega - n\Omega - k_{zs}u/\gamma)} + \frac{wJ_n^2(k_{\perp s}w/\gamma\Omega)}{\gamma(\omega - n\Omega - k_{zs}u/\gamma)^2}\left[k_{zs}^2 - \frac{(n\gamma\Omega + k_{zs}u)^2}{\gamma^2c^2}\right]\right\}, \tag{12}$$

where $[J_n^2(x)]'=d[J_n{}^2(x)]/dx$. This result can be found in an early unpublished report by Bers and Speck [16] and can be obtained by algebraic rearrangement from a formula published by Chen and Chu [17]. For a cold electron beam, with $f_0(u,w)=(N/2\pi W)\delta(w-W)\delta(u-U)$, Eq. (12) leads to

$$1=\frac{\omega_p^2}{W^2}\sum_{n=-\infty}^{\infty}\frac{1}{k^2}\left\{\frac{nk_{\perp s}W[J_n^2]'}{(\omega-n\Omega-k_{zs}U/\gamma)}+\frac{W^2J_n^2}{\gamma(\omega-n\Omega-k_{zs}U/\gamma)^2}\times\left[k_{zs}^2-\frac{(n\gamma\Omega+k_{zs}U)^2}{\gamma^2c^2}\right]\right\}, \quad (13)$$

where $J_n^2=J_n^2(k_{\perp s}W/\gamma\Omega)$.

A preliminary appraisal of the nature of the roots of Eq. (13) can be found by assuming that waves associated with each value of n in the series are decoupled and that $k_{\perp s}^2 \gg k_{zs}^2$. Equation (13) for each n is then of the form

$$(\omega-n\Omega-k_{zs}U/\gamma)^2-A_n(\omega-n\Omega-k_{zs}U/\gamma)-B_n(k_{zs})=0\ , \quad (14)$$

where

$$A_n=\frac{\omega_p^2}{k^2W}nk_{\perp s}[J_n^2]'\ ,$$

$$B_n(k_{zs})=\frac{\omega_p^2}{k^2\gamma}[J_n^2]\left[k_{zs}^2-\frac{(n\gamma\Omega+k_{zs}U)^2}{\gamma^2c^2}\right].$$

In practice the coefficients A_n and $B_n(k_{zs})$ are much smaller than unity, in which case, Eq. (14) has the approximate solution

$$k_{zs}\approx\frac{\gamma}{U}\left\{\omega-n\Omega-\frac{A_n}{2}\mp\left[\frac{A_n^2}{4}+B_n(k_{zs})\right]^{1/2}\right\}$$

$$\approx\frac{\gamma}{U}\left[\omega-n\Omega\mp B_n^{1/2}\left[\frac{\gamma(\omega-n\Omega)}{U}\right]\right], \quad (15)$$

since usually $A_n^2 \ll 4B_n$. Equation (15) admits complex conjugate values of k_{zs} for real ω in the frequency interval where B_n is negative, namely,

$$\frac{n}{1+\beta_z}\le\frac{\omega}{\Omega}\le\frac{n}{1-\beta_z}\ , \quad (16)$$

where $\beta_z=U/\gamma c$. The maximum imaginary value of k_{zs} occurs at

$$\omega=\frac{n\Omega}{1-\beta_z^2}$$

and is given by

$$[\mathrm{Im}(k_{zs})]_{\max}\approx\frac{\omega_p}{c}\frac{\beta_\perp}{\beta_z\gamma^{1/2}}\left[\frac{1}{1-\beta_z^2}\right]^{1/2}\frac{nJ_n(k_{\perp s}\rho_g)}{(k_{\perp s}\rho_g)}\ , \quad (17)$$

where $\beta_\perp=W/\gamma c$ and $\rho_g=W/\gamma\Omega$. Equation (16) shows that the frequency interval where gain is associated with the harmonic term n overlaps that associated with the term $(n+1)$ when $n\ge(1-\beta_z)/2\beta_z$.

It is easy to show that the reduced dispersion relation Eq. (14) corresponds to convective instability (i.e., spatial amplification) for waves moving in the same direction as the beam in the frequency range given by Eq. (16). This follows [18] since in this range real ω corresponds to complex k_{zs}, while real k_{zs} corresponds to complex ω.

Equation (17) can be recast to give the maximum value of the power amplification coefficient, namely,

$$[G_s^{(n)}]_{\max}=20(\log_{10}e)[\mathrm{Im}(k_{zs})]_{\max}=0.1331\alpha f_n\left[\frac{I}{\gamma\beta_z(1-\beta_z^2)(R_2^2-R_1^2)}\right]^{1/2}\ \mathrm{dB/cm}\ , \quad (18)$$

where I is the beam current in amperes, $\alpha=\beta_\perp/\beta_z$ is the velocity ratio, $f_n=\max[nJ_n(k_{\perp s}\rho)/(k_{\perp s}\rho)]$, and R_1 and R_2 are measured in cm. Figure 4 shows plots of f_n and the corresponding values of $x_n=(k_{\perp s}\rho)$, as functions of n. As an example, for $n=10$, one has $f_n=0.261$ and $x_n=11.44$. Table I shows parameters as predicted by Eq. (18) for a hypothetical tenth harmonic gyroamplifier with single-mode operation based on these values. Since $k_{\perp s}\rho=11.4$ for this example, it is seen that the approximation is justified that the excitations given by Eq. (8) are essentially periodic in r. For the cases discussed, the coaxial inner spacing of 1.8 mm is between 3 and 4 gyration radii, so that the beam can almost be considered "thick" in comparison with conventional gyrotron annular beams. It is assumed that such a thickness is adequate to support space charge dominated Bernstein modes, but this point deserves further study.

The parameters of Table I are not intended as the basis for a device design, but rather to demonstrate that the small-signal gain levels that can be estimated for an amplifier operating near 300 GHz with relatively low values of operating voltage, current, and magnetic field are significant enough to warrant a detailed numerical analysis. Such an analysis is presented in the next section of this paper.

IV. NUMERICAL EXAMPLES

In this section of the paper, selected examples are chosen for numerical evaluation of the spatial growth

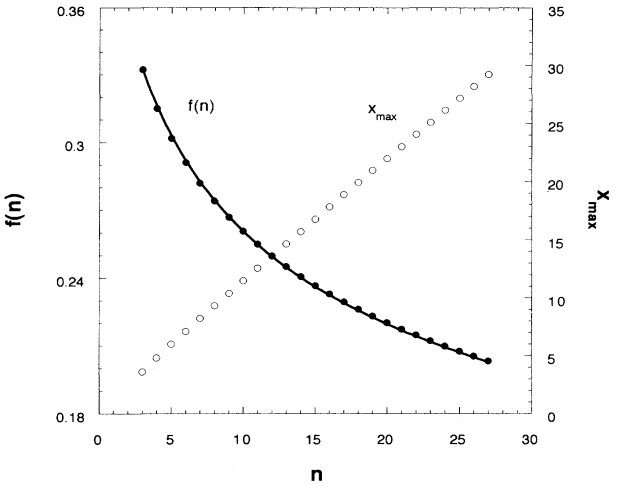

FIG. 4. Maximum growth factor $f_n(n)$ and $x_{max}(n)$ versus harmonic index n.

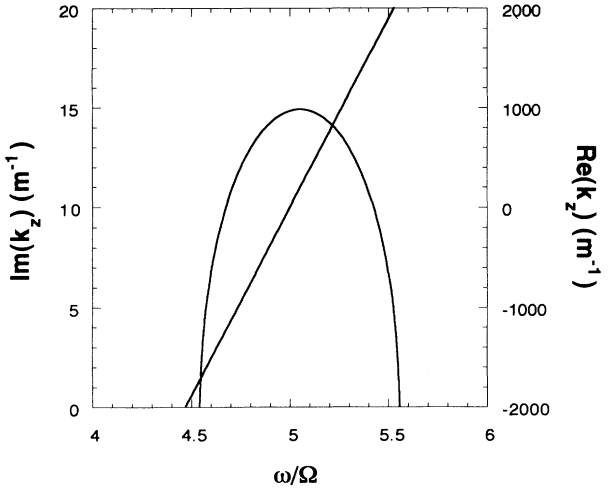

FIG. 5. $\mathrm{Re}(k_z)$ (straight line) and $\mathrm{Im}(k_z)$ (curve) versus ω/Ω near the fifth harmonic for $s=13$, for a 30-kV, 8-A beam with $\alpha=2.0$.

rates as given by the roots of Eq. (13) for a cold beam and Eq. (12) for a beam with finite axial velocity spread. Most solutions that are given assume that terms under the summation signs in each equation decouple from one another. This assumption is tested in two examples by solving for roots when nearest-neighbor terms to the dominant term are also included. Solutions are shown for a specified value of $k_{\perp s}$ in each case as well, assuming that a means exists for coupling to only one radial beam mode. A possible means for effecting this selective coupling is described in Sec. V.

Results for the first example as shown in Figs. 5–10 are for a fifth harmonic amplifier. In this case a 30-kV, 8-A beam with $\alpha=2.0$ is chosen. For a cold beam, Fig. 5 shows the solutions found from the $n=5$ term of Eq. (13) for the real and imaginary parts of k_z, as functions of ω/Ω. In this figure, results are shown for the 13th radial mode, which is the mode that has the peak gain. The peak value for $\mathrm{Im}(k_z)$ of 14.9 m^{-1} (1.3 dB/cm) agrees to better than 2 parts in 10^5 with the value predicted by Eq. (17). These values indicate that a fifth harmonic, 140-GHz amplifier could be built requiring a magnetic field of only 10.58 kG. Figure 6 shows solutions for $\mathrm{Im}(k_z)$ for radial modes between the 9th and 18th, so that the relative gain values for each of these can be compared. It is seen that seven modes ($s=9$, 10, 11, 12, 14, 15, and 16) have peak gain values greater than half that for the fastest growing mode $s=13$. Figure 7 shows solutions from the $n=4$, 5, and 6 terms in Eq. (13) for $s=13$, evaluated from taking one term at a time from under the summation and from taking three terms. The solutions in this case are seen to be virtually identical, even where gain spectra from the fifth and sixth terms overlap. Figure 8 shows the gain spectra obtained from finding roots for the first eight terms under the summation for $s=13$, taken one term at a time. The result shows that gain is obtained continuously in frequency over a considerable bandwidth. The relative magnitudes of the gain arising from different n values is a function of radial mode index s; for a higher value of s, the peak gain occurs for higher n. Clearly it will be necessary to devise a means of selecting a given s value so as to optimize the gain spectrum for a given application.

TABLE I. Parameters for a hypothetical tenth harmonic amplifier, at five different values of B, corresponding to excitations of the five radial eigenvalues $10 \le s \le 15$ as listed, at the five center frequencies also as listed. The small-signal peak gain value of 2.16 dB/cm predicted by Eq. (18) is the same for all five cases.

beam voltage	30 kV
beam current I	8.0 A
velocity ratio α	2.0
inner coax radius R_1	0.06 cm
outer coax radius R_2	0.24 cm
harmonic index n	10
radial eigenvalue $k_{\perp s}R_1$	10.48, 11.53, 12.57, 13.62, 14.67, 15.71
magnetic field B (kG)	8.09, 8.90, 9.71, 10.52, 11.33, 12.13
gyration radius ρ_g (mm)	0.65, 0.60, 0.55, 0.50, 0.47, 0.44
center frequency (GHz)	214, 235, 257, 278, 299, 321
peak small-signal gain	2.16 dB/cm

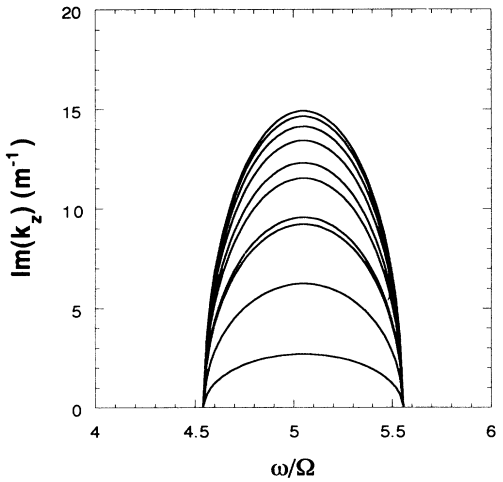

FIG. 6. Im(k_z) versus ω/Ω near the fifth harmonic for several values of radial mode number s, for a 30-kV, 8-A beam with $\alpha=2.0$. From the bottom up, $s=18$, 17, 9, 16, 10, 15, 11, 14, 12, and 13.

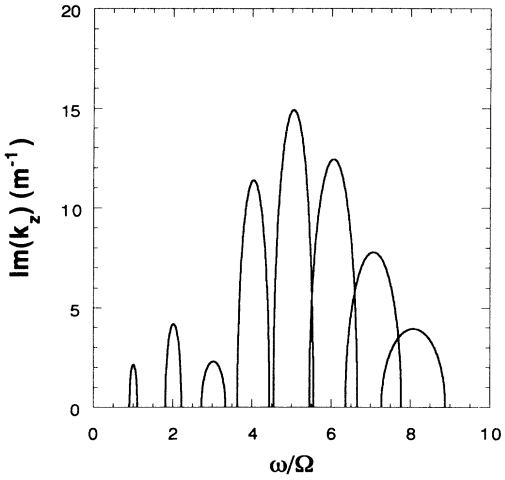

FIG. 8. Gain spectrum Im(k_z) for the first eight terms of the dispersion relation, taken one term at a time, for the same beam as in Figs. 5–7.

Figure 9 shows the effect of axial velocity spread on gain for $s=13$. In this case, Eq. (12) has been evaluated (using the $n=5$ term alone) for a distribution of axial velocities given by the flat-top function

$$f(u)=\frac{1}{\Delta u}\left[H\left[u-u_0+\frac{\Delta u}{2}\right]-H\left[u-u_0-\frac{\Delta u}{2}\right]\right], \tag{19}$$

where $H(x)=1$ for $x>0$, $H(x)=0$ for $x<0$, and Δu is the full width at half maximum of $f(u)$. The gain curves in Fig. 9 are seen to narrow with increasing axial velocity spread, since the growth for larger values of k_z is more severely affected than for smaller k_z. (Growth for zero k_z is not affected by velocity spread.) To examine the sensitivity of the gain dependence on velocity spread to the form of the distribution function, a second distribution was also used in evaluating Eq. (12), namely, the Maxwellian distribution

$$f(u)=\frac{2}{\Delta u}\left[\frac{\ln 2}{\pi}\right]^{1/2}\exp\left\{-4\ln 2\left[\frac{u-u_0}{\Delta u}\right]^2\right\}, \tag{20}$$

where again Δu is the full width at half maximum for $f(u)$. The results, shown in Fig. 10 for $\Delta u/u_0=4\%$, are seen to be essentially the same as for the distribution given by Eq. (19). From the curves shown in Fig. 9, it appears that velocity spread values of less than about 5%

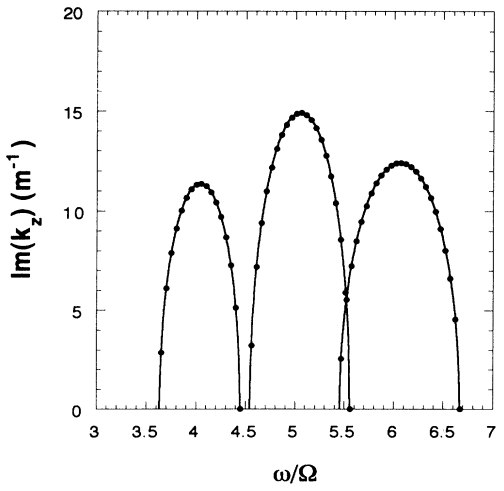

FIG. 7. Comparison for Im(k_z) between one-term (solid curves) and three-term (dots) solutions of the dispersion relation for $s=13$ for the same beam as in Figs. 5 and 6.

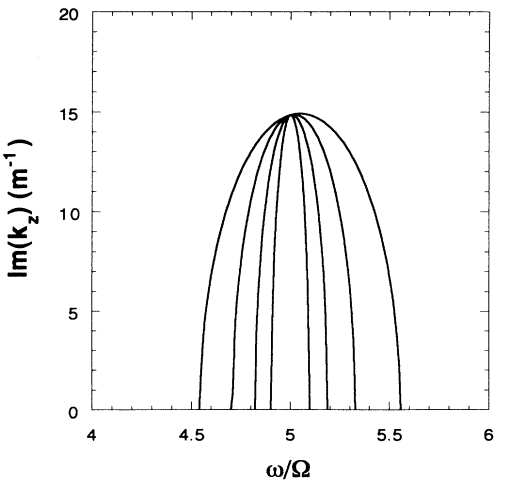

FIG. 9. Effect of velocity spread on gain curve for the fifth harmonic term. From the wide to the narrow curves, values of $\Delta u/u$ are 0, 2.0%, 4.0%, 6.0%, and 8.0%, respectively.

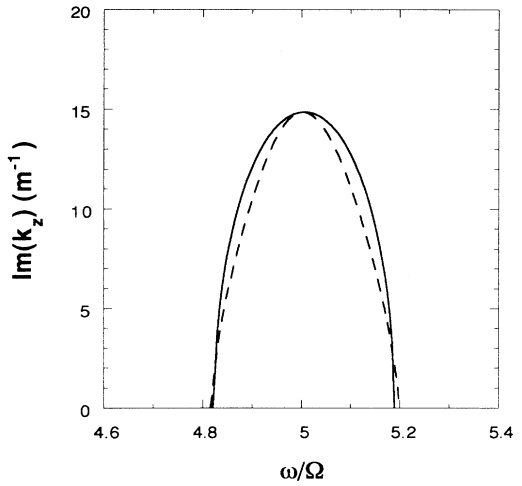

FIG. 10. Comparison of gain curve for $\Delta u/u$ of 4.0%, using a uniform distribution [Eq. (19), solid curve] and a Gaussian distribution [Eq. (20), dashed curve] of equal full width at half maximum velocities.

are needed in order to preserve significant bandwidth in a fifth harmonic device.

Figures 11–13 are for tenth harmonic operation using the same structure as in the example given in Table I, with $R_2=4R_1=0.240$ cm. Figure 11 shows evaluations of (a) $\mathrm{Im}(k_z)$ and (b) $\mathrm{Re}(k_z)$ from Eq. (13) for the terms $n=9$, 10, and 11 for a 10-kV, 2-A beam having $\alpha=3.0$. From the curves for $\mathrm{Re}(k_z)$ shown in Fig. 11(b) one sees that, generally, phase matching [i.e., specification of both ω/Ω and $\mathrm{Re}(k_z)$] selects a gain curve corresponding to only a single n term. The condition for phase matching can be made quantitative by equating $\mathrm{Re}(k_z)$ as found from Eq. (15) to its value for the TE_{11} mode of the interior cylindrical waveguide, namely, $[(\omega/c)^2-(1.841/R_1)^2]^{1/2}$. Frequencies where this matching can occur are thus given by solutions of the quadratic equation

$$\left[\frac{\omega}{n\Omega}\right]^2(1-\beta_z^2)-2\left[\frac{\omega}{n\Omega}\right]+1+\left[\frac{1.841c\beta_z}{n\Omega R_1}\right]^2=0\ , \tag{21}$$

where $\beta_z=U/c\gamma$. The last term on the right-hand side of Eq. (21) can be written $(1.841/n\alpha)^2(\rho/R_1)^2$, which for $n=10$ and $\alpha=3.0$ becomes $3.766\times10^{-3}(\rho/R_1)^2$. Since, for tenth harmonic operation, the optimum eigenvalue of $k_\perp R_1$ is 14.67 (14th radial mode) and since, from Fig. 4, the gain has its peak value for $k_\perp\rho=11.44$, one finds $\rho/R_1=0.780$. The last term in Eq. (21) is thus seen to reduce to a numerical factor 2.29×10^{-3}. As a result, one sees from Eq. (21) that the two values of $\omega/n\Omega$ where exact phase matching occur are determined only by β_z. For a 10-kV beam having $\alpha=3.0$, the $n=10$ solutions of Eq. (21) are $\omega=9.65\Omega$ and 10.43Ω. The low frequency root corresponds to a wave with negative k_z, i.e., one traveling in the negative z direction, while the high frequency root corresponds to a wave traveling in the positive z direction. Table II summarizes the results for this model tenth harmonic gyroamplifier.

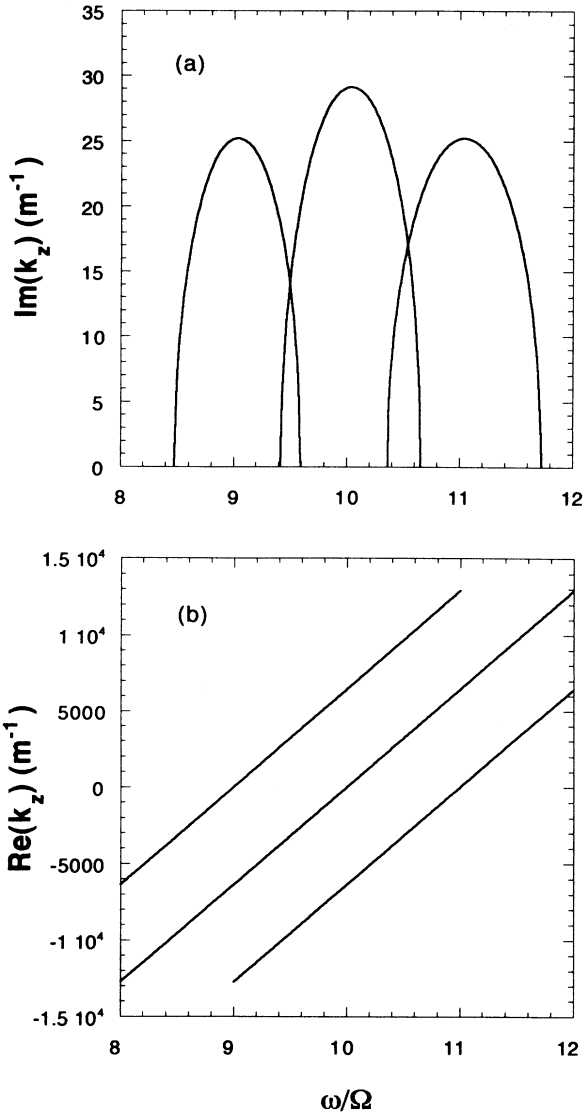

FIG. 11. (a) $\mathrm{Im}(k_z)$ and (b) $\mathrm{Re}(k_z)$ versus ω/Ω near the tenth harmonic, where the evaluations are taken from only one term of the dispersion relation. For beam parameters, see Table II.

TABLE II. Parameters for a hypothetical tenth harmonic amplifier, when phase matching exists between the growing beam mode ($s=14$) and the copropagating TE_{11} mode in the interior waveguide. The axial velocity spread value is calculated from Eq. (6).

beam voltage	10 kV
beam current I	2 A
beam perveance	2×10^{-6} A V$^{-3/2}$
velocity ratio α	3
inner coax radius R_1	0.06 cm
outer coax radius R_2	0.24 cm
harmonic index n	10
radial mode index s	14
magnetic field B	6.87 kG
axial velocity spread	1.51%
small signal gain G	2.53 dB/cm
center frequency	188.6 GHz

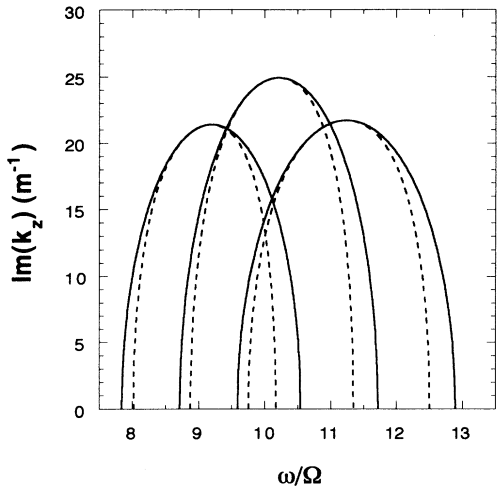

FIG. 12. Comparison for $\mathrm{Im}(k_z)$ between one-term solutions (solid curves) and three-term solutions (dashed lines) of the dispersion relation for $s=14$ for a 30-kV, 8-A beam with $\alpha=2.0$.

Figure 12 compares results for the gain spectrum calculated from the $n=9$, 10, and 11 terms of the dispersion relation [Eq. (13)] taken one term at a time (solid lines) and taken together (dashed lines). For this example and that depicted in Fig. 13, the beam voltage is increased to 30 kV to increase the overlap between the gain curves. Other parameters for these examples are $\alpha=2.0$, $I=8\,A$, $B=11.3$ kG, and $s=14$. As compared with results near the fifth harmonic (Fig. 7) where overlap between neighboring terms is nearly absent, one sees in Fig. 12 a distinct difference between solutions obtained from one term and from three terms of Eq. (13). With a significant overlap of gain curves at the higher harmonics, this example suggests that evaluations taken one term at a time could introduce measurable error. (This observation may extend to other high harmonic gyrointeractions as well.)

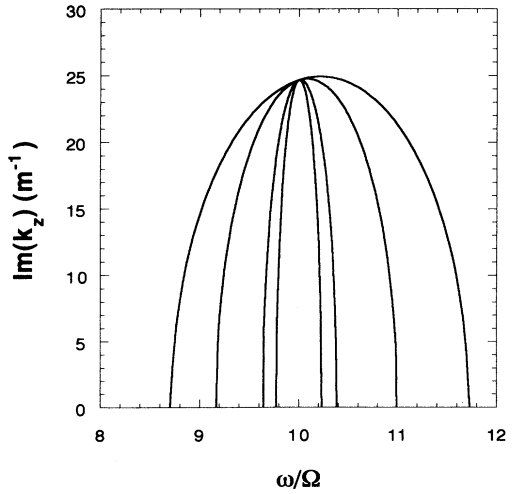

FIG. 13. Effects of axial velocity spread on gain spectrum near the tenth harmonic for a 30-kV, 8-A beam with $\alpha=2.0$. The outer curve is for zero velocity spread, while the inner curves are for $\Delta u/u=1.0\%$, 3.0%, and 5.0%, respectively.

Figure 13 shows the effect of axial velocity spread on the gain spectrum calculated from the $n=10$ term of the dispersion relation alone. The curves shown are for $\Delta u/u=0$, 1.0%, 3.0%, and 5.0% in sequence, with zero velocity spread having the widest bandwidth, as in Fig. 9. But, in this case, the narrowing is seen to be greater at smaller velocity spread values than for the fifth harmonic example shown in Fig. 9. For tenth harmonic operation, one can surmise that velocity spread values of less than about 2% should be tolerable.

V. CONCEPTUAL DEVICE CONFIGURATION

The theory and numerical results presented above suggest that a millimeter-wave amplifier could, in principle, be built based on the gyroharmonic convective instability for electrostatic waves on a coaxial electron beam. The parameters given in Table II for a hypothetical tenth harmonic 189-GHz amplifier are indeed remarkable, as regards the low voltage, current, and magnetic field required, in comparison with proposed fast-wave gyroamplifiers [19]. But several irksome problems that arise from the nature of the rich spectrum of electrostatic modes that the beam can support need to be discussed. In this brief section of the paper, these problems will be reviewed and a device configuration that could mitigate against them will be presented.

The eigenfunctions for small-signal disturbances on the beam are given by Eq. (7). The analysis presented in this paper was for the dipole mode, corresponding to $m=1$. Clearly, a parallel analysis can be carried out for any value of m, corresponding to higher-order multipole modes. For these, convective instability at the gyroharmonics occurs as well, with a spectrum of $k_{\perp s}$ given by solution of an equation similar to Eq. (9), but with J_m and Y_m in place of J_1 and Y_1; this spectrum will be different from that for the dipole mode. But even if only the dipole mode is excited, it has been shown that significant growth exists for a range of s-values. In the example shown in Fig. 6, peak gain values greater than half that for the peak mode with $s=13$ are exhibited for eight different radial modes at the same frequency. These modes can have axial wave numbers k_{zs} that are nearly the same, so it would be possible to avoid serious destructive phase interference between the modes. But, if the input signal is shared between the design mode ($s=13$, say) and other modes with lesser growth, the overall gain of the amplifier will be diminished from the value anticipated for $m=1$, $s=13$ alone. Moreover, if the input signal is coupled partially to modes that are not growing, an input coupling loss will result to further diminish the overall gain of the amplifier. As a result, a practical gyroamplifier configuration will have to include means to suppress modes with undesired values of m and s.

One possible device configuration that could mitigate against the problems described in the preceding paragraph is shown schematically in Fig. 14. Only the output

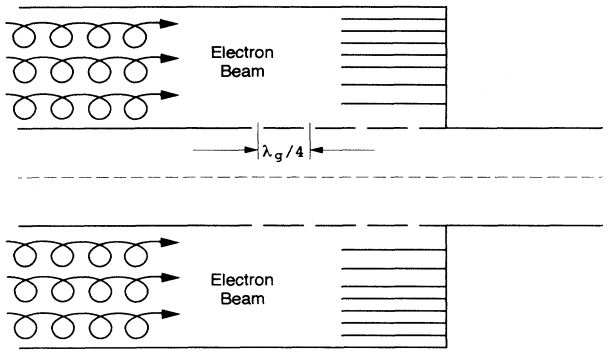

FIG. 14. Conceptual device design, showing the region near output coupler with coaxial vane structure intended to suppress unwanted radial modes. Coupling holes between interior TE_{11} waveguide and coaxial region are spaced azimuthally by 180° and axially by one-quarter guide wavelength to allow preferential coupling to the dipole mode with phase matching between the electrostatic and electromagnetic waves.

end of the interaction region is shown in the figure; a similar input end would be some distance off the figure to the left. The central cylindrical axial pipe is the electromagnetic waveguide, designed to propagate only the lowest TE_{11} mode. Coupling holes separated in azimuth by 180° allow the radial electric field with polarization directed between the holes to penetrate into the coaxial region containing the electron beam, thereby preferentially exciting the dipole mode in the beam. The coupling holes are spaced axially by one-quarter guide wavelength in both the cylindrical and coaxial waveguides, ensuring phase matching along the coupling region preferentially for the dipole mode. Even-m multipole modes would have opposite polarity at points differing in azimuth by 180° and thereby should not be excited with a field such as the TE_{11}. At each end of the coaxial waveguide, a nest of cylindrical vanes could be inserted; seven such vanes are shown in Fig. 14. These vanes would be positioned at some or all of the potential nodes for the design mode and therefore provide an axial boundary condition at the input and output locations that does not short out any of the electric field lines of the design mode. The vanes would, however, cut electric field lines of competing radial modes, whose potential nodes would be at other radii, and thus could serve to suppress these modes. One technical issue that arises in the implementation of this mode suppression strategy is the relatively small physical scale: for the example given in Table II, the vanes need to be fitted into an annulus of radial gap equal to 0.18 cm. This could pose a challenge, especially at the collector end of the device, where the beam power is absorbed. An alternate scheme (not shown in the figure) could involve the inverse boundary structure, namely, a set of nested cylinders, with gaps located at radii where the desired mode's axial electric field is zero. In any case, it is clear that some form of mode suppression should be employed at the input and output couplers to allow energy to flow only into and out of the desired beam mode.

Mode selection notwithstanding, another quirk of this interaction surrounds its behavior for waves traveling counter to the direction of beam flow. (These will be termed "backward waves" for purposes of this discussion.) For specificity, reference will be made to Fig. 11. One sees, at $\omega/\Omega=9.5$, for instance, that the backward wave associated with the $n=10$ term of the dispersion relation has nearly the same spatial growth rate as does the forward wave associated with the $n=9$ term. A similar phenomenon is seen at $\omega/\Omega=10.5$ involving the backward wave from $n=11$ and the forward wave from $n=10$. This effect can occur whenever $n \geq (1-\beta_z)/2\beta_z$, as was shown from Eq. (16). Whenever the gain curves from adjacent n values overlap, growth will occur for waves traveling both with, and counter to, the direction of beam flow. This increases the round-trip gain for a wave reflected from the far end of the amplifying region in the device and sets a more stringent requirement for impedance matching at the input coupler to avoid oscillations. (Oscillations can occur if the round-trip gain minus the circuit losses exceed the reflection coefficient at the input coupler.) Only at frequencies equal to half-integer harmonics will the forward and backward waves have equal magnitude axial wave numbers. The result of having gain for co- and countertraveling waves can be an advantage, in that a single-coupler reflection amplifier can be conceived of with larger gain than otherwise possible. But, as described above, increased precautions may have to be exercised to avoid undesirable oscillations.

VI. CONCLUSIONS

Analysis and numerical results have been presented for the growth of small amplitude waves on a coaxial electron beam flowing between conducting cylinders in a uniform guide magnetic field. This configuration has been shown to make possible a gyroharmonic millimeter-wave amplifier that would not require high beam voltages or high magnetic fields. Coaxial geometry has been shown to embody at least two important virtues. These are (a) lower potential depression than for a cylindrical beam of equal perveance, and thus lower irreducible axial velocity spread, and (b) access to the beam fields for coupling at an interior surface. For beam perveance of 2×10^{-6} $A\,V^{-3/2}$ or below, axial velocity spread [1.5%, as calculated from Eq. (6) for $\alpha=3$ and $R_2=4R_1$] has been shown to not seriously affect the small-signal gain. The interior access permits coupling to the radial electrostatic fields at the interior beam edge through periodic holes that allow phase matching to TE_{11} lowest mode electromagnetic fields of input and output couplers.

It has been shown that the beam can support spatially growing waves with short radial scale lengths, so that strong wave-particle coupling exists at high gyroharmonics even for a low voltage beam. In an example cited for a tenth harmonic amplifier at 188.6 GHz, use of a 10-kV, 2-A beam in a 6.86-kG magnetic field was shown to lead to a small-signal growth rate of 2.53 dB/cm. A 25-dB amplifier would be of the order of 10 cm long if gain is supported in a single pass or only about 5 cm long if round-trip gain can be achieved, neglecting input cou-

pling loss. If an efficiency of 5% could be realized with this device, it would result in an extremely compact kilowatt-level amplifier with operating parameters that are much more modest than other devices currently under development. For analysis of high harmonic gain, where overlap between adjacent terms occurs, it has been shown to be necessary to evaluate the dispersion relation including terms neighboring the term closest to the harmonic of interest if errors are to be avoided.

The analysis presented in this paper has invoked linearization procedures that do not allow a strict conclusion to be drawn on the nonlinear saturation level for the interaction. However, an estimate of the saturation level can be found by reference to Eq. (17), where the linearized spatial amplification rate is seen to be essentially proportional to $J_n(k_{\perp s}\rho_g)$, since β_z is nearly constant and $\gamma \approx 1$ changes but slightly. As the beam particles give up transverse momentum to the fields, $\rho_g = c\beta_\perp/\Omega$ will decrease. We can estimate the condition for saturation by identifying the value $(\gamma\beta_\perp)_{1/2}$, which causes $J_n(k_{\perp s}\rho_g)$ to fall to half its initial value. Thus we approximate

$$\gamma_{\rm sat} = \left[\frac{1+(\gamma\beta_\perp)^2_{1/2}}{1-\beta_z^2} \right]^{1/2} \tag{22}$$

and

$$\eta = \frac{\gamma_0 - \gamma_{\rm sat}}{\gamma_0 - 1} , \tag{23}$$

where η is the efficiency at saturation and γ_0 is the initial energy factor. Applying this approximate analysis to the tenth harmonic examples given in Tables I and II, where $(\gamma\beta_\perp)_{1/2}/(\gamma_0\beta_{\perp 0}) = 0.793$, gives η to be 29.7% and 33.3%, respectively, corresponding to power outputs of 71 and 6.7 kW for the two hypothetical devices.

Several important issues unique to the electrostatic gyroharmonic mode of amplification on the beam require additional study. These center on means of suppressing undesired azimuthal and radial modes that, if excited, would probably lead to a diminution in device gain. One configuration that could mitigate against the undesired modes has been suggested in this paper. The assumption invoked that the infinite medium dispersion relation applies for a beam of thickness 3–4 gyroradii needs to be evaluated. Additionally, it is essential to explore nonlinear aspects of the interaction systematically, both for understanding of physics issues that may arise when more than one mode is excited and for obtaining accurate values of device efficiency and saturated gain.

ACKNOWLEDGMENTS

Stimulating discussions were held with A. K. Ganguly. This work was supported by the U.S. Army Research Office and the U.S. Naval Research Laboratory.

[1] I. B. Bernstein, Phys. Rev. **109**, 10 (1957); D. E. Baldwin, I. B. Bernstein, and M. P. H. Weenink, *Advances in Plasma Physics 3,* edited by A. Simon and W. B. Thompson (Interscience, New York, 1969), pp. 87–95.
[2] J. L. Hirshfield, Bull. Am. Phys. Soc. **37**, 1537 (1992); J. L. Hirshfield and P. Bershatsky, *ibid.* **38**, 1999 (1993).
[3] J. L. Hirshfield, Phys. Lett. A **167**, 383 (1992).
[4] J. L. Hirshfield, Int. J. Infrared Millimeter Waves **2**, 695 (1981).
[5] Z. Liang, N. A. Ebrahim, and J. L. Hirshfield, J. Infrared Millimeter Waves **4**, 423 (1983).
[6] N. A. Ebrahim, Z. Liang, and J. L. Hirshfield, Phys. Rev. Lett. **49**, 1556 (1982).
[7] N. A. Ebrahim, Z. Liang, and J. L. Hirshfield, Bull. Am. Phys. Soc. **28**, 1194 (1983).
[8] H. Li and T. M. Antonsen, Jr., Phys. Plasmas **1**, 714 (1994).
[9] G. Landuaer, J. Nucl. Energy C **4**, 395 (1962).
[10] F. W. Crawford, G. S. Kino, and H. H. Weiss, Phys. Rev. Lett. **13**, 229 (1964).
[11] F. W. Crawford, J. Res. Natl. Bur. Stand. Sec. D **69**, 789 (1965).
[12] E. G. Harris, J. Nucl. Energy C **2**, 138 (1961).
[13] L. Brillouin, Phys. Rev. **67**, 260 (1945).
[14] A. W. Trivelpiece and R. W. Gould, J. Appl. Phys. **30**, 1784 (1959).
[15] *Handbook of Mathematical Functions,* edited by M. Abramovitz and I. A. Stegen (Dover, New York, 1972), p. 374.
[16] A. Bers and C. E. Speck, MIT Research Laboratory of Electronics Report No. 78, 1965 (unpublished).
[17] K. R. Chen and K. R. Chu, IEEE Trans. Microwave Theory Tech. **MTT-34**, 72 (1986).
[18] See, for example, A. I. Akhiezer *et al.*, *Collective Oscillations in a Plasma* (MIT Press, Cambridge, MA, 1967), pp. 96–109.
[19] G. S. Park *et al.*, IEEE Trans. Plasma Sci. **22**, 536 (1994).